analytical chemistry

pubs.acs.org/ac Article

Zinc–Metal Organic Frameworks: A Coreactant-free Electrochemiluminescence Luminophore for Ratiometric Detection of miRNA-133a

Xiaoyan Wang, Siyu Xiao, Changping Yang, Congyi Hu, Xue Wang, Shujun Zhen, Chengzhi Huang,* and Yuanfang Li*

Cite This: *Anal. Chem.* 2021, 93, 14178–14186 Read Online

ACCESS | Metrics & More | Article Recommendations | Supporting Information

ABSTRACT: Developing a coreactant-free ratiometric electrochemiluminescence (ECL) strategy based on a single luminophore to achieve more accurate and sensitive microRNA (miRNA) detection is highly desired. Herein, utilizing zinc–metal organic frameworks (Zn-MOFs) as the single luminophore, a novel dual-potential ratiometric ECL biosensor was constructed for ultrasensitive detection of miRNA-133a. The as-prepared Zn-MOFs exhibited simultaneous cathode and anode ECL emission. Furthermore, the Zn-MOFs were confirmed to be a multichannel ECL sensing platform with excellent annihilation and coreactant ECL emission. The corresponding ECL behaviors were investigated in detail. Benefiting from the hybridization chain reaction (HCR) amplification technology, *N*,*N*-diethylethylenediamine (DEAEA) was modified on hairpin DNA, and the gained products loaded with quantities of DEAEA enhanced the anodic ECL intensity of Zn-MOFs. In the presence of miRNA-133a, the ECL intensity ratio of anode to cathode (I_a/I_c) was significantly increased, which realized the ultrasensitive ratiometric detection of miRNA-133a. In addition, without an exogenous coreactant, the biosensor revealed superb accuracy and stability. Under optimal conditions, the detection linearity of miRNA-133a was from 50 aM to 50 fM with a low detection limit of 35.8 aM (S/N = 3). This is the first work to use Zn-MOFs as a single emitter for reliable ratiometric ECL bioanalysis, which provides a new perspective for fabricating a ratiometric ECL biosensor platform.

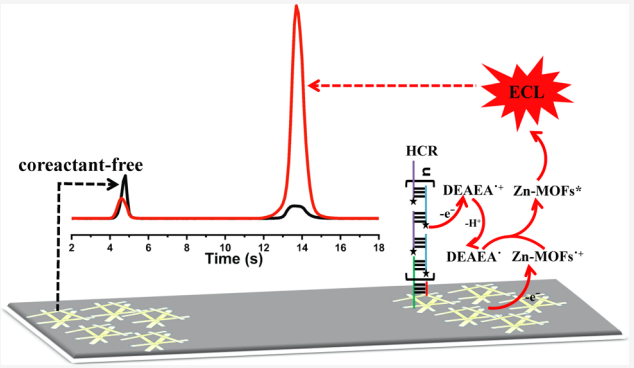

INTRODUCTION

On its virtues of low background, high sensitivity, simple operation, and fast response, electrochemiluminescence (ECL) has received lots of attention in biosensing.[1−3] Unfortunately, ECL biosensors usually rely on changes in a single signal to operate; false positives or negatives may occur on account of other interferences, particularly in a complex analytical system. The strategy to solve this defect is mainly to develop ratiometric ECL biosensors through the built-in correction of the signals of the two luminophores.[4] Generally, biosensors including dual-wavelength ratiometric and dual-potential ratiometric properties are mainly constructed. A dual-wavelength biosensor is a kind of biosensor in view of the ECL resonance energy transfer between two wavelength-dependent luminophores.[5] Recently, many new dual-wavelength ECL biosensors have been successfully exploited.[6−10] Nevertheless, for dual-wavelength ratiometric ECL biosensors, an ECL spectrometer or filter is usually needed. However, the ECL spectrometer mainly collects signals through CCD; the output ECL signal value is relatively low. Since the filter only allows partial wavelengths of light to pass through, it also has a great influence on the final output ECL signal. These make them less sensitive than expected.[11] Another strategy is to construct a dual-potential ratiometric ECL, which requires a cathode and anode emitter and can emit light independently in a wide potential range. Xu's team reported the first dual-potential ratiometric ECL biosensor, utilizing luminol and CdS quantum dots as anode and cathode emitters, respectively, to achieve sensitive detection of DNA.[11] After that, many dual-potential ratiometric ECL biosensors have been developed.[12−14] However, the reported ratiometric ECL strategy mostly needs two eligible luminophores, which increased the complexity of the ECL systems and severely restricted applications.

Received: July 8, 2021
Accepted: September 28, 2021
Published: October 12, 2021

https://doi.org/10.1021/acs.analchem.1c02881
Anal. Chem. 2021, 93, 14178−14186

Scheme 1. (A) Synthesis of Zn-MOFs and (B) Illustration of the Coreactant-Free Ratiometric ECL Biosensor for Detecting miRNA-133a

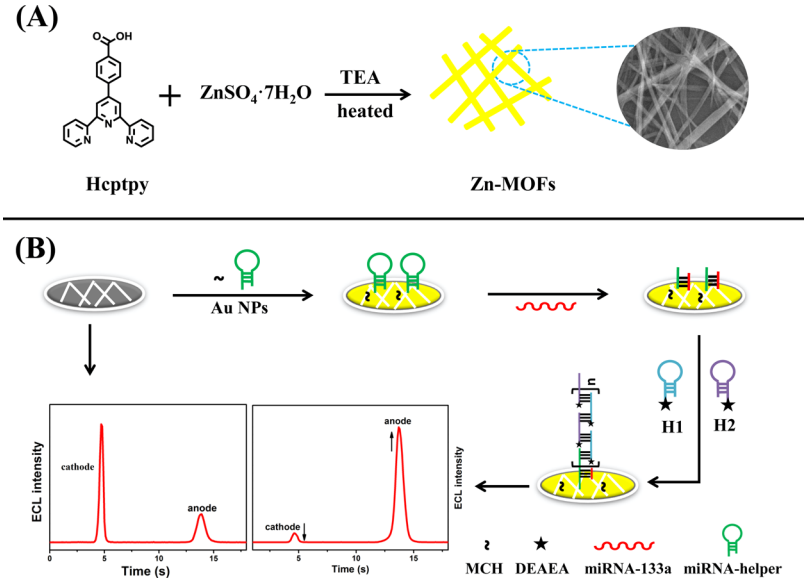

In recent years, a number of ratiometric ECL biosensors have been developed using a single emitter. For instance, Xia's team discovered that using graphene quantum dot as the single emitter, a ratiometric ECL strategy was gained through the chemical and electrochemical reactions of $K_2S_2O_8$ and Na_2SO_3 and realized sensitive detection of human IgG.[15] Wang's group proposed another ratiometric ECL biosensor based on luminol as a single emitter and H_2O_2 as an effective coreactant to realize the sensitive detection of carcinoembryonic antigens.[16] Dong's team developed a ratiometric ECL biosensor by utilizing RuNDs as a single luminophore in the presence of BPQDs as the anodic coreactant and $K_2S_2O_8$ as the cathodic coreactant for the detection of tumor marker mucin 1.[17] However, in order to obtain an excellent ECL signal, at least one suitable coreactant needs to be added in the above-mentioned ratiometric strategies. The addition of the coreactant would affect the detection environment, resulting in poor stability of the ECL system and causing measurement errors.[18,19] To avoid the flaws of externally adding coreactants, the following methods have been taken: (a) utilizing the dissolved oxygen in the detection system as a coreactant;[20,21] (b) enzyme-catalyzed in situ generation of coreactants;[22] and (c) a self-enhanced ECL system was prepared by integrating an emitter and a coreactant in the same framework structure or complexes.[23,24] The above mentioned strategies could indeed enhance the luminescence stability of the emitter, but there are still some shortcomings. First, when dissolved oxygen was utilized as the coreactant, the unclear concentration of dissolved oxygen would inevitably lead to measurement data errors and poor reproducibility. Second, the conditions of use of the enzyme were very harsh, which limited its application range. Then, the method of integrating the luminophores and the coreactant into a molecular structure was cumbersome and difficult to operate. Hence, it is so meaningful to exploit a single ECL luminophore that does not require a coreactant and synthesized by a simple method under conventional experimental conditions.

Organic luminophores have been widely researched and developed in ECL systems due to their unique advantages of structural tailorability, high quantum yield, and adjustable light emission wavelength.[25] However, for most organic molecules with a poor solubility in the water phase, the luminescence signal lacked sufficient stability and usually attenuated. Metal–organic frameworks (MOFs) are a kind of molecular crystalline materials constructed by connecting metal centers and bridging organic ligands.[26−28] They have unique framework structure characteristics, higher ECL intensity, more stable ECL signals, and lower ECL potential than organic luminescence ligands.[29,30]

MicroRNAs (miRNA's) are a short-chain, endogenous expression of noncoding RNA molecules that regulate gene expression at the post-transcriptional level and play an important role in regulating key biological processes.[31] MiRNA-133a is considered as a biomarker for acute myocardial infarction (AMI). The expression of miRNA-133a in the blood of patients is significantly increased when AMI occurs.[32] It is very essential to realize its low abundance detection. Thus, utilizing 4′-(4-carboxyphenyl)-2, 2′:6′, 2″-terpyridine (Hcptpy) as the organic luminescence ligand and zinc as the metal node, we obtained a novel ECL nanoluminophore named Zn-MOFs through a simple one-pot hydrothermal method (Scheme 1A). Annihilation and coreactant ECL behaviors of Zn-MOFs were investigated in detail. With the above mentioned considerations, a new dual-potential ECL biosensor based on Zn-MOFs as the single luminophore was constructed for the ratiometric detection of miRNA-133a without adding any coreactant. As exhibited in Scheme 1B, Zn-MOF films on the glassy carbon electrode (GCE) were used as a detection platform which could perform a dual-potential ECL emission. Then, the miRNAhelper was assembled on the surface of the GCE by the Au–S bonds. Furthermore, with increasing concentrations of miRNA-133a, the abundant *N*,*N*-diethylethylenediamine (DEAEA) introduced by the hybridization chain reaction (HCR) was used to enhance the ECL intensity of Zn-MOFs. Thus, a high sensitivity and accuracy for detection of miRNA-133a was achieved through this ratiometric ECL biosensor. This work provides hope for the development of a coreactant-free

https://doi.org/10.1021/acs.analchem.1c02881
Anal. Chem. 2021, 93, 14178−14186

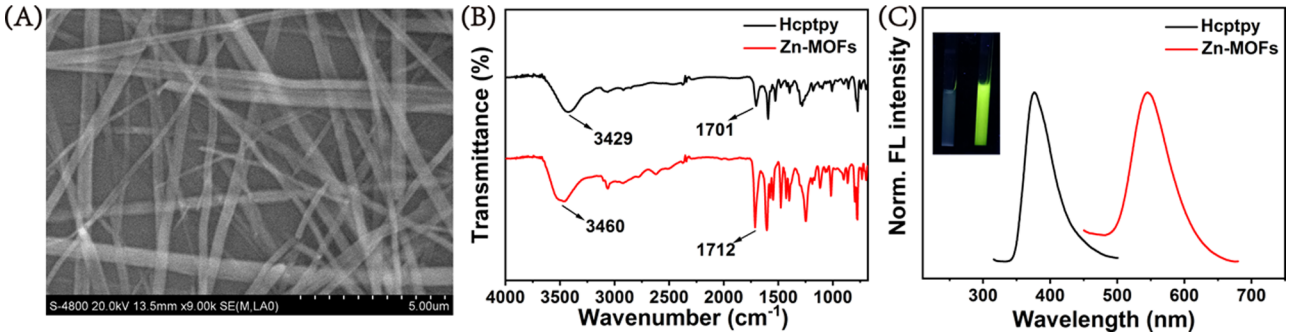

Figure 1. (A) SEM images of Zn-MOFs. (B) FT-IR spectra of the Hcptpy ligand and Zn-MOFs. (C) FL spectrum of Hcptpy and Zn-MOFs. Inset: photograph of the Hcptpy (left) and Zn-MOF (right) suspension with 365 nm UV light illumination.

ratiometric biosensor using MOFs as a single ECL luminophore.

EXPERIMENTAL SECTION

Reagents and Apparatus. The reagents and apparatus are supplemented in the Supporting Information. The nucleic acid sequence is shown in Table S1.

Synthesis of Zn-MOFs. The Zn-MOFs were synthesized by a hydrothermal method by following our group's previously reported literature with slight modification.[33] In brief, 0.1 mmol Hcptpy was dispersed in 9 mL of H_2O and triethylamine (TEA) was used to help dissolve it. At the same time, 0.1 mmol $ZnSO_4{\cdot}7H_2O$ was dissolved in 1 mL of H_2O. Then, 9 mL of Hcptpy solution and 1 mL of $ZnSO_4{\cdot}7H_2O$ solution were mixed completely. After that, the mixture was thermally treated at 120 °C in a Teflon-lined stainless-steel autoclave for 24 h. After cooling down to room temperature, the yellow nanocrystals were harvested by centrifuging (8000 rpm, 5 min) and washed twice with *N*,*N*-dimethylformamide and ultrapure water, respectively. At last, the Zn-MOFs were lyophilized and dispersed in ultrapure water for the following use.

Preparation of DEAEA-Labeled Hairpin DNA. DEAEA and H1 were cross-linked through 1-ethyl-3-(3-dimethylaminopropyl)-carbodiimide hydrochloride (EDC) and hydroxylsuccinimide sodium salt (NHS) through the literature previously reported by our group.[34] Briefly, H1 (100 μL, 5 μM) was activated by EDC (30 μL, 1.5 M) and NHS (30 μL, 0.35 M) for 2 h. Then, DEAEA (40 μL, 0.1 M) was added to the activated H1 and incubated overnight at 37 °C. Finally, DEAEA-labeled H1 was gained. Likewise, DEAEA-labeled H2 was prepared through the abovementioned steps except that H1 was replaced.

Native PAGE. Prior to the HCR, the miRNA helper, H1, and H2 were heated to 95 °C for 5 min and then kept at 25 °C for 2 h. Then, miRNA-133a (10 fM), miRNA helper (1 μM), H1 (1 μM), and H2 (1 μM) were mixed and incubated for 75 min. The hydrogel (12%) was prepared by mixing 2.4 mL of 40% acrylamide/diacrylamide gel solution (29:1), 1.6 mL of 5× TBE buffer solution, 56 μL of 10% ammonium persulfate (APs), 8 μL of *N*,*N*,*N*′,*N*′-tetramethylenediamine (TEMED), and 4 mL of deionized water.[35] After mixing the samples with loading buffer, they were added into the gel electrophoresis channel. Subsequently, the electrophoresis was run at a constant voltage of 120 V for about 72 min and the gel was stained in ethidium bromide solution for 15 min. Finally, the electrophoresis photograph was gained using an imaging system.

Electrode Modification and Ratiometric Biosensor Fabrication. First, the bare GCE (Φ = 3 mm) was burnished carefully in sequence with 0.3 and 0.05 μm alumina powders. Then, in order to acquire a flawless electrode surface, the bare GCE was sonicated in H_2O and ethanol for 5 min, respectively. After that, 5 μL of Zn-MOFs (1 mg/mL) and 5 μL of gold nanoparticle (Au NP) solutions were dropped onto the surface of the pretreated electrodes and dried. Subsequently, 8 μL of miRNA-helper (1 μM) was dropped on the electrode surface and reacted overnight at 4 °C. Furthermore, nonspecific binding sites were blocked by MCH solution (5 μL, 1 mM). Following this, miRNA-133a (8 μL) solutions of different concentrations were placed onto the modified electrode surface and reacted at 37 °C for 90 min. At last, H1 (4 μL, 1 μM) and H2 (4 μL, 1 μM) were spread on the surface of the electrode and reacted at 37 °C for 90 min. After each step of the modification, the electrode was carefully rinsed with phosphate buffer saline (PBS) buffer for three times. Finally, the fabricated biosensor was detected in PBS buffer (0.1 M, pH 7.4). The potential scanning range covered from −1.5 to 1.3 V with a scan rate of 0.3 V/s.

RESULTS AND DISCUSSION

Characterization of the As-Prepared Zn-MOFs. The morphology was characterized by scanning electron microscopy (SEM), which showed a typical fibrous structure (Figure 1A). The diameter size of the synthesized Zn-MOFs was about 100 nm to 700 nm. The Fourier transform infrared (FT-IR) spectra of Hcptpy and Zn-MOFs are exhibited in Figure 1B. The shoulder peaks at 3429 and 1701 cm^{-1} assigned to carboxyl and carbonyl groups in Hcptpy were shifted to 3460 and 1712 cm^{-1}, respectively, showing the successful coordination of carbonyl and Zn^{2+}. Additionally, the characteristic peak at about 1600−1300 cm^{-1} of the pyridine ring in Hcptpy was also found in Zn-MOFs, while a slight peak shift and increase in intensity were observed, revealing the coordination of Zn^{2+} and nitrogen in Hcptpy. It has been previously reported that Hcptpy-based self-assembled metal coordination polymers were coordinated with O-donor and N-donor ligands,[33,36] which was consistent with our hypothesis that Zn^{2+} coordination of carbonyl and tripyridyl groups forms Zn-MOFs (Figure S1). The fluorescence (FL) spectrum (Figure 1C) showed the ligand Hcptpy with a maximum emission wavelength of 376 nm under an excitation wavelength of 281 nm. Light-blue FL of Hcptpy was obtained under a 365 nm UV lamp (Figure 1C, left of the inset). However, when the Zn-MOFs formed, the maximum FL emission peak shifted to 545 nm at an excitation wavelength of 284 nm. The yellow-green

https://doi.org/10.1021/acs.analchem.1c02881
Anal. Chem. 2021, 93, 14178−14186

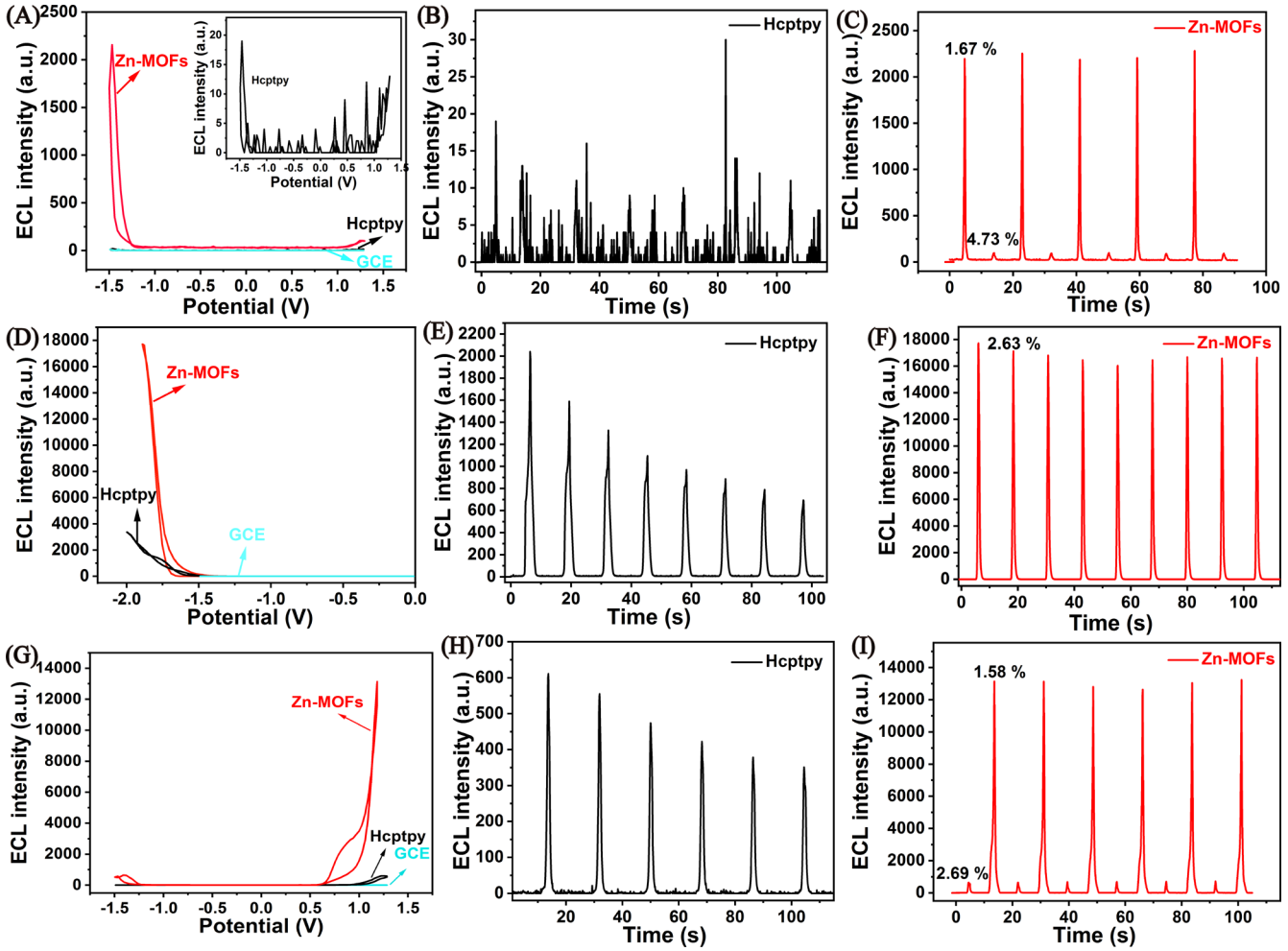

Figure 2. (A–C) ECL responses of different modified electrodes in PBS (0.1 M, pH 7.4). (D–F) ECL signals of different modified electrodes in PBS (0.1 M, pH 7.4) containing 10 mM $K_2S_2O_8$. (G), (H), and (I) ECL curves of different modified electrodes in PBS (0.1 M, pH 7.4) containing 10 mM TPrA.

FL of Zn-MOFs was observed under a UV lamp at 365 nm (Figure 1C, right of the inset). Powder X-ray diffraction (PXRD) was utilized to confirm the crystal structure of Zn-MOFs (Figure S2), which showed similar PXRD with the simulated pattern.[37] All of the results demonstrated the successful synthesis of Zn-MOFs.

ECL Performance of Zn-MOFs. In order to study the excellent multichannel ECL emission of Zn-MOFs, the ECL intensity of different modified electrodes, including bare GCE, Hcptpy, and Zn-MOFs, was first investigated without adding any coreactant. As shown in Figure 2A, almost no ECL intensity was obtained on the bare GCE. The ECL intensity of Hcptpy at the cathode and anode was very weak. Only Zn-MOFs possessed strong anode and cathode ECL signals. Meanwhile, the ECL intensity of Hcptpy was weak and unstable through continuous scanning (Figure 2B). However, the Zn-MOFs could maintain a good stability and the ECL signals of the cathode and anode almost had no attenuation with relative standard deviations (RSDs) of 1.67 and 4.73%, respectively (Figure 2C). The main reason was that after the organic ligand Hcptpy was coordinated with zinc, Zn-MOFs were formed and acted as new luminophores. Its maximum emission peak had changed, and the luminescence performance had become stronger.[23] The stability of Zn-MOFs in aqueous solution was relatively good. Under multiple electrical excitations, the frame structure of Zn-MOFs remains unchanged and the Zn-MOFs would not fall off from the electrode.[30] MOFs have a stronger emission center than ligands. Thus, Zn-MOFs were a more stable and efficient luminophore than Hcptpy. In addition, the ECL response of Zn-MOFs dispersed in aqueous solution was continuously investigated for 10 days (Figure S3). The ECL responses of the cathode and anode almost remained unchanged with RSDs of 2.72 and 4.43%, respectively.

Subsequently, an outstanding ECL response was obtained in the presence of $K_2S_2O_8$ as the cathode coreactant. The ECL intensity of bare GCE, Hcptpy, and Zn-MOFs was compared in PBS (0.1 M, pH 7.4) containing 10 mM $K_2S_2O_8$ (Figure 2D). Both Hcptpy and Zn-MOFs could generate cathode ECL signals. However, although the ECL response of Hcptpy reached about 3400 a.u. at the beginning, the intensity decayed radically until it became very weak (Figure 2E), which was very unfriendly for the application. Conversely, the Zn-MOFs exhibited a very strong ECL response (about 17,500 a.u.), and the observed ECL intensity was stable over a long period of repeated cycles with an RSD of 2.63% (Figure 2F). This exhibited the ECL strength, and the stability of Zn-MOFs was significantly improved than Hcptpy in the presence of $K_2S_2O_8$.

Furthermore, the ECL intensity of bare GCE, Hcptpy, and Zn-MOFs was compared in PBS (0.1 M, pH 7.4) containing

https://doi.org/10.1021/acs.analchem.1c02881
Anal. Chem. 2021, 93, 14178−14186

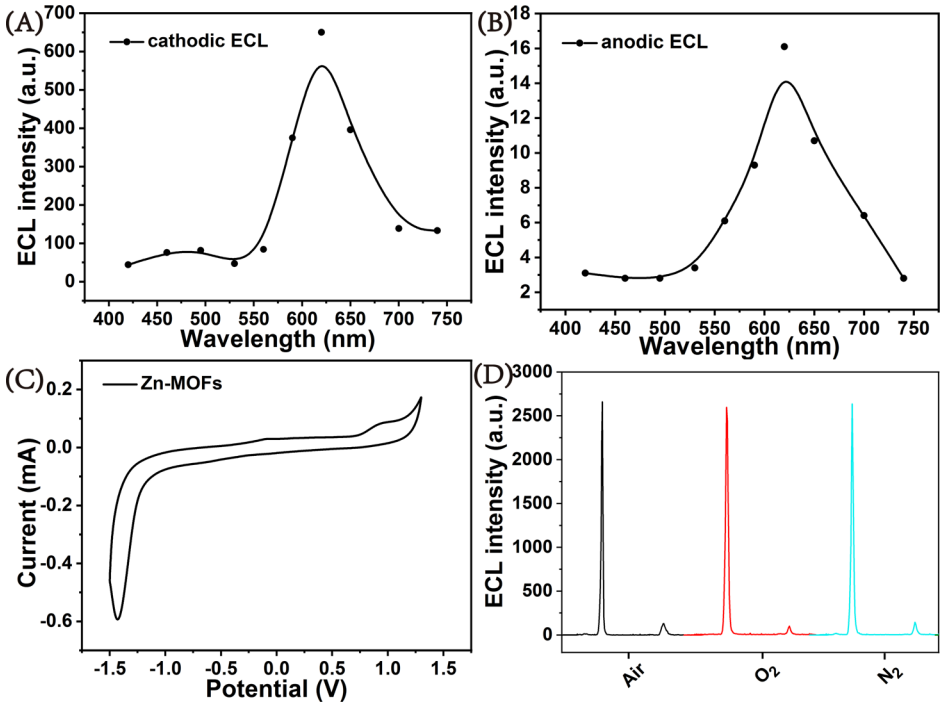

Figure 3. ECL spectra for the Zn-MOFs/PBS system at cathode potential (A) and anode potential (B) using optical filters. (C) CV curves of Zn-MOFs in PBS (0.1 M, pH 7.4). (D) ECL response of Zn-MOFs modified GCE with air and saturated O2 and N2 in PBS.

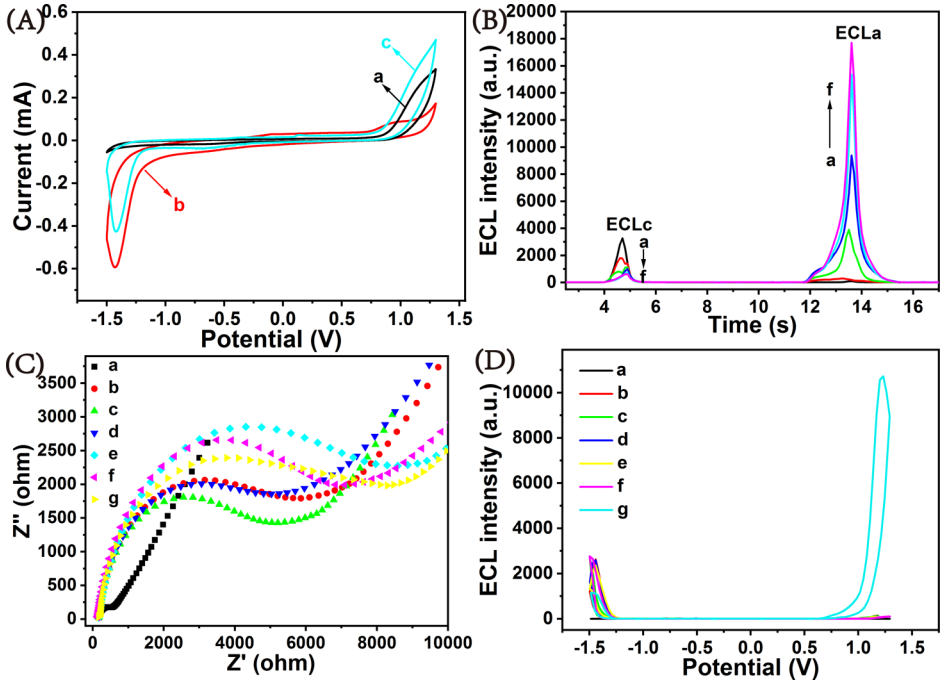

Figure 4. (A) CV curves of DEAEA (curve a), Zn-MOFs (curve b), and Zn-MOFs/DEAEA system (curve c) in PBS (0.1 M, pH 7.4). (B) ECL signals of Zn-MOFs in 0.1 M PBS (pH 7.4) solution including different concentrations of DEAEA (from a to f: 0, 0.5, 2, 5, 8, and 10 mM). (C) EIS and (D) ECL responses of GCE (a), GCE/Zn-MOFs (b), b/Au NPs (c), c/miRNA-helper (d), d/MCH (e), e/miRNA-133a (f), and f/H1/H2 (g). EIS was investigated in 0.1 M KCl solution containing 5 mM $[Fe(CN)_6]^{3-/4-}$.

10 mM TPrA (Figure 2G). Since TPrA can effectively promote the anodic ECL signal of the emitter, an obvious anodic ECL signal of Hcptpy was observed, while the cathodic ECL signal was too weak to be observed. Meanwhile, TPrA could also effectively enhance the anodic ECL signal of Zn-MOFs and only slightly reduce the cathode ECL signal. In the stability experiment, the ECL response of Hcptpy could reach about 600 a.u. at the beginning, but the intensity decayed gradually and the signal was not stable (Figure 2H). On the contrary, Zn-MOFs maintained a steady ECL signal during continuous scanning, with RSDs of 2.69% to the cathode and 1.58% to the anode (Figure 2I). In brief, compared with Hcptpy, Zn-MOFs exhibited stronger ECL emission, better stability, and wider potential window.

https://doi.org/10.1021/acs.analchem.1c02881
Anal. Chem. 2021, 93, 14178−14186

ECL Mechanism. To study the coreactant-free ECL emission mechanism of the Zn-MOFs, we need to identify the emitter in this ECL system. The ECL spectra of Zn-MOFs at cathode and anode potential were observed using the optical filter(Figure 3A,B). This displayed that the ECL emission peaks appeared at a cathode potential of 620 nm and an anode potential of 622 nm. Both the ECL emission peaks exhibited a visible red shift in contrast to the FL emission peak (545 nm), which demonstrated that the excited state of Zn-MOF* for ECL emission might be mainly dependent on more sensitive surface state transitions.[38] To further elucidate the cathode and anode ECL mechanism of Zn-MOFs, cyclic voltammogram (CV) curves of Zn-MOFs were investigated (Figure 3C). The Zn-MOFs displayed a strong reduction peak at about −1.4 V and a weak oxidation peak at about 0.9 V by injecting or extracting electrons. Meanwhile, the reduction current was much greater than the oxidation current of Zn-MOFs, indicating that its oxidation state was more stable.[39] In addition, the effect of dissolved oxygen on ECL intensity was examined, as shown in Figure 3D, and there was no difference either in air or oxygen-saturated and nitrogen-saturated PBS. These results showed that dissolved oxygen could not affect the ECL response of Zn-MOFs.

Based on the above mentioned discussion, we proposed the possible ECL emission mechanism for the coreactant-free ECL system. First, Zn-MOFs could be oxidized and reduced during the potential cycling. The electrochemical reduction of Zn-MOFs generated Zn-MOFs$\dot{s}^-$ radicals (eq 1). The electrochemical oxidation of Zn-MOFs occurred and generated Zn-MOFs$\dot{s}^+$ radicals (eq 2). The generated Zn-MOFs$\dot{s}^+$ radicals subsequently collided with Zn-MOFs$\dot{s}^-$ radicals to produce Zn-MOFs* by the electron-transfer annihilation process (eq 3). Finally, a strong cathode ECL and weak anode ECL emission occurred as the excited state returns to the ground state to release energy (eq 4). In a word, the corresponding coreactant-free ECL mechanism could be described in the following equations

$$\text{Zn-MOFs} + e^- \rightarrow \text{Zn-MOFs}^{\cdot -} \quad (1)$$

$$\text{Zn-MOFs} - e^- \rightarrow \text{Zn-MOFs}^{\cdot +} \quad (2)$$

$$\text{Zn-MOFs}^{\cdot -} + \text{Zn-MOFs}^{\cdot +} \rightarrow \text{Zn-MOFs}^* \quad (3)$$

$$\text{Zn-MOFs}^* \rightarrow \text{Zn-MOFs} + h\nu \quad (4)$$

Principle of the Proposed Ratiometric ECL Biosensor. DEAEA is a small molecule with a similar structure to TEA, which was reported that it could enhance the ECL signal of Au nanoclusters.[40] Therefore, in this work, DEAEA was introduced into this coreactant-free ECL system through HCR to enhance the anode ECL intensity of Zn-MOFs. As exhibited in Figure 4A, CV curves of DEAEA, Zn-MOFs, and Zn-MOFs/DEAEA in PBS (0.1 M) were investigated. Only a reversible oxidation peak was observed in DEAEA. The Zn-MOFs displayed a strong reduction peak at the cathode and a weak oxidation peak at the anode in PBS buffer. However, upon the addition of DEAEA, the oxidation potential of Zn-MOFs shifted and the current remarkably increased. The reduction peak of Zn-MOFs did not change significantly, just the current was decreased, indicating that DEAEA mainly affected the oxidation of Zn-MOFs at the anode but had little effect on the reduction of Zn-MOFs at the cathode. Then, DEAEA of different concentrations was detected in the Zn-MOFs/PBS system (Figure 4B). The cathode ECL signal decreased slightly, while the anodic ECL intensity increased markedly as the concentration of DEAEA increased, manifesting that DEAEA could act as an effective anodic enhancer. The weak change in cathode ECL might be caused by the competitive-mechanism-driven ECL process of anodic ECL. Specifically, Zn-MOFs could be electrochemically oxidized to produce Zn-MOF$\dot{}^+$ radicals. DEAEA could be oxidized to generate DEAE$\dot{A}^+$. Then, the DEAE$\dot{A}^+$ could undergo deprotonation to generate DEAE$\dot{A}$. Following that, Zn-MOFs$\dot{s}^+$ could be reacted with DEAE$\dot{A}$ to form more Zn-MOFs* and then emitted an ECL signal during its relaxation process. Equations 5−9 described the possible anode mechanism of the Zn-MOFs/DEAEA ECL system

$$\text{Zn-MOFs} - e^- \rightarrow \text{Zn-MOFs}^{\cdot +} \quad (5)$$

$$\text{DEAEA} - e^- \rightarrow \text{DEAEA}^{\cdot +} \quad (6)$$

$$\text{DEAEA}^{\cdot +} \rightarrow \text{EADEAEA}^{\cdot} + H^+ \quad (7)$$

$$\text{Zn-MOFs}^{\cdot +} + \text{DEAEA}^{\cdot} \rightarrow \text{Zn-MOFs}^* \text{ (more)} \quad (8)$$

$$\text{Zn-MOFs}^* \rightarrow \text{Zn-MOFs} + h\nu \quad (9)$$

Moreover, only Zn-MOFs act as the emitter in this system, so the cathode ECL signal would be competitive by the anode ECL signal. The electrochemical oxidation of Zn-MOFs was observed and generated less Zn-MOF$\dot{}^+$ radicals. Thus, the cathode ECL signal of the Zn-MOF was reduced. Equations 10−13 described the possible cathode mechanism of the Zn-MOFs/DEAEA ECL system

$$\text{Zn-MOFs} + e^- \rightarrow \text{Zn-MOFs}^{\cdot -} \quad (10)$$

$$\text{Zn-MOFs} - e^- \rightarrow \text{Zn-MOFs}^{\cdot +} \text{ (less)} \quad (11)$$

$$\text{Zn-MOFs}^{\cdot -} + \text{Zn-MOFs}^{\cdot +} \rightarrow \text{Zn-MOFs}^* \text{ (less)} \quad (12)$$

$$\text{Zn-MOFs}^* \rightarrow \text{Zn-MOFs} + h\nu \quad (13)$$

To verify the feasibility of the HCR, the as-prepared samples were analyzed by polyacrylamide gel electrophoresis (PAGE) (Figure S4). The lanes from 1 to 9 were relative to the miRNAhelper, H1, H2, miRNA-133a, H1 + H2, miRNA-133a + H1 + H2, miRNA-helper + miRNA-133a, miRNAhelper + H1 + H2, and miRNAhelper + miRNA-133a + H1 + H2. When incubated miRNA-133a, miRNAhelper, H1, and H2, a battery of bands was observed (lane 9), showing that this HCR was effectively triggered. Furthermore, Au NPs with electronegativity might be adsorbed by electropositive Zn-MOFs (Figure S5). Electrochemical impedance spectroscopy (EIS) was used for the stepwise preparation of the proposed ratiometric ECL biosensor (Figure 4C). The semicircular part of EIS was related to the electron transfer resistance (Ret), related to the difficulty of electron transfer of a ferricyanide-redox probe between the electrode and the solution.[41,42] Because the electroactive ions are transported rapidly to the electrode interface, a very small semicircle was acquired from the bare GCE (curve a). After Zn-MOFs were modified onto the GCE, the Ret increased duo to the poor conductivity of Zn-MOFs (curve b). On account of good conductivity of Au NPs, Ret decreased after Au NPs were dripped onto the Zn-MOFs/GCE surface (curve c). The impedance increased after the miRNA helper modified onto the electrode surface, which showed an unfavorable environment for electron transfer (curve d). After assembling MCH, a bigger Ret was observed since interfacial charge transfer was blocked (curve e).

https://doi.org/10.1021/acs.analchem.1c02881
Anal. Chem. 2021, 93, 14178−14186

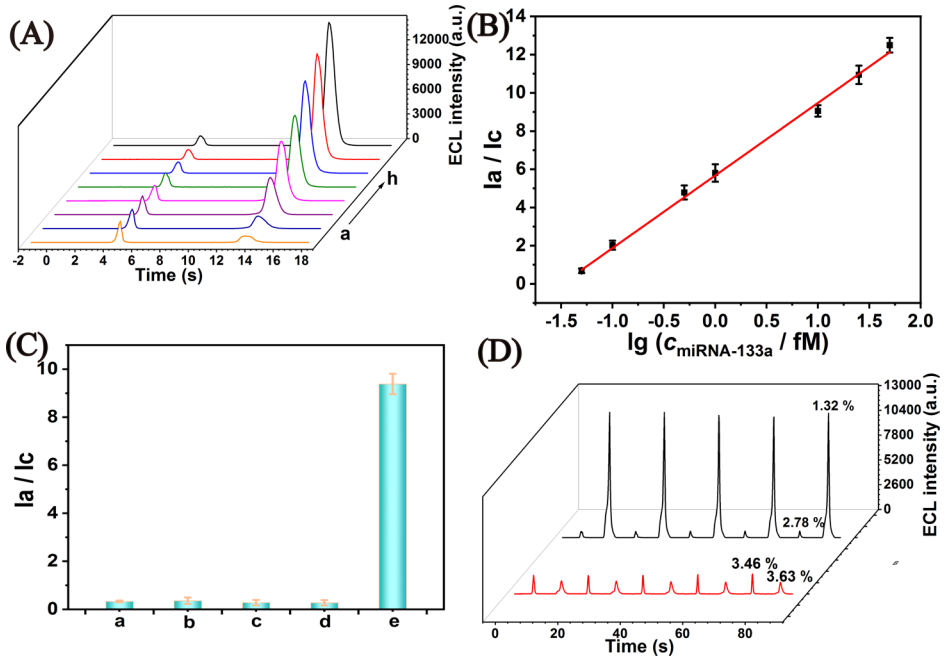

Figure 5. (A) ECL intensity−time curves for the ratiometric ECL biosensor toward miRNA-133a (the concentrations from a to h: 0, 0.05, 0.1, 0.5, 1, 10, 25, and 50 fM). (B) Calibration curve of I_a/I_c vs lg cmiRNA-133a. (C) Selectivity of this ratiometric ECL biosensor with different miRNAs: (a) blank, (b) miRNA-21 (1 pM), (c) miRNA-107 (1 pM), (d) miRNA-141 (1 pM), and (e) miRNA-133a (10 fM). (D) Stability of the ratiometric ECL biosensor with 50 aM and 25 fM miRNA-133a.

However, when miRNA-133a was assembled onto the electrode surface (curve f), the Ret decreased, which was ascribed to the hydrophilicity and rigidity of the DNA duplex that caused DNA to reside further from the electrode surface and the interface electron transfer was promoted. After assembling HCR, because of the steric hindrance effect, the Ret was increased (curve g). Thus, these EIS results clearly demonstrated the successful construction of the biosensor. In addition, the ECL characterization was measured during the construction process (Figure 4D). There was no obvious ECL signal on the bare GCE (curve a). Similar ECL signals were observed with a stronger cathode ECL intensity and a weaker anode ECL intensity (curves b, c, d, e, and f), originating from luminescence of Zn-MOFs. Only after the HCR was incubated, the biosensor exhibited a slightly reduced cathode ECL and a marked strong anode ECL (curve g). Hence, the DEAEA-labeled DNA could be applied to implement ratiometric ECL for miRNA-133a assay.

Analytical Ability of the Proposed Ratiometric Biosensor. So as to obtain the excellent detection performance, a series of related factors including the concentration of Zn-MOFs, the incubation time of miRNA-133a and HCR, the pH value of the PBS buffer, and the content of Au NPs were optimized. The best concentration of Zn-MOFs was 1.0 mg/mL (Figure S6). The appropriate incubation time for miRNA-133a was 75 min (Figure S7). The most suitable incubation time of HCR was 90 min (Figure S8). The best pH environment of PBS buffer was 7.4 (Figure S9). The optimal volume of Au NPs was 5 μL (Figure S10).

The analytical ability of this biosensor was investigated. The correlation between the I_a/I_c ratio and the logarithmic concentration of miRNA-133a was evaluated. As displayed in Figure 5A, I_c decreased gradually and I_a increased rapidly as the concentration of miRNA-133a increased. As a result, I_a/I_c increased, enabling the ratiometric detection of miRNA-133a. As exhibited in Figure 5B, the ECL signals exhibited a good linearity over the logarithmic concentration of miRNA-133a ranging from 50 aM to 50 fM. The equation of linear regression for the proposed bioassay was $I_a/I_c = 5.67 + 3.80 \lg (c_{133a}/\text{fM})$ with a correlation coefficient of $R^2 = 0.9972$. The limit of detection (LOD) was calculated to be 35.8 aM (S/N = 3). Other miRNA-133a detection methods are listed in Table S2 and compared with this bioassay method. The excellent analytical properties of miRNA-133a could be ascribed to the efficient HCR amplification process. Due to the reverse trend of the two ECL signals, the signal ratio was more explicit, thereby greatly reducing the probability of false positives/false negatives.

To assess the selectivity of this biosensor, three different noncomplementary oligonucleotides including miRNA-21, miRNA-141, and miRNA-107 were tested. As displayed in Figure 5C, these interfering substances caused no significant change to the I_a/I_c ratio compared with the blank sample. A remarkable I_a/I_c ratio increased after the addition of miRNA-133a (10 fM), showing that this biosensor had good selectivity for miRNA-133a. Furthermore, the one-base mismatched, two-base mismatched, and three-base mismatched sequence as target RNA was also used to evaluate the specificity of the proposed method (Figure S11). Seven sensing platforms were fabricated under the same environment; 1 fM miRNA-133a was selected to measure their ECL intensities (Figure S12). The RSD of cathode ECL was 6.39% and the RSD of anode ECL was 1.75%, revealing that the ratiometric ECL biosensor possessed a favorable reproducibility. In addition, 50 aM and 25 fM miRNA-133a were chosen to evaluate the stability of this biosensor. As shown in Figure 5D, all the RSDs decreased by 5%, demonstrating that the ratiometric ECL strategy displayed an excellent stability.

In order to verify the practical application of the detection system, we applied it to the detection of miRNA-133a in

https://doi.org/10.1021/acs.analchem.1c02881
Anal. Chem. 2021, 93, 14178−14186

human serum. The standard addition method was used to verify the accuracy of the method, and the results are shown in Table S3. The recoveries ranged from 99.2 to 104.9%, and the relative errors and RSDs were very low, exhibiting a good practicality for the clinical detection of miRNA-133a.

CONCLUSIONS

In summary, utilizing the prepared Zn-MOFs as a single luminophore, cathode and anode ECL emission of Zn-MOFs was simultaneously observed. The annihilation and coreactant ECL emission of Zn-MOFs were investigated. A coreactant-free ratiometric ECL biosensor was developed based on the presence of DEAEA-connected hairpin DNA for ultrasensitive miRNA-133a detection. The ratiometric strategy obtained notable improvements in ECL intensity, stability, accuracy, and sensitivity. In view of these excellent ECL performances, this work not only provides a novel way to explore high quality ECL luminophores for their unique systems but also greatly expands the perspective for the design of a novel single luminophore for the ratiometric ECL biosensors.

ASSOCIATED CONTENT

Supporting Information

The Supporting Information is available free of charge at https://pubs.acs.org/doi/10.1021/acs.analchem.1c02881.

Reagents and apparatus; characterization of Zn-MOFs; PAGE characterization of the HCR system; optimization experiment; selectivity and reproducibility of the biosensor; sequences of the nucleic acids; comparison of different methods for miRNA-133a detection; and real blood sample analysis (PDF)

AUTHOR INFORMATION

Corresponding Authors

Chengzhi Huang − *Key Laboratory of Luminescent and Real-Time Analytical System (Southwest University), Chongqing Science and Technology Bureau, College of Pharmaceutical Sciences, Southwest University, Chongqing 400715, P. R. China*; orcid.org/0000-0002-1260-5934; Email: chengzhi@swu.edu.cn

Yuanfang Li − *Key Laboratory of Luminescence Analysis and Molecular Sensing (Southwest University), Ministry of Education, College of Chemistry and Chemical Engineering, Southwest University, Chongqing 400715, P. R. China*; orcid.org/0000-0001-5710-4423; Email: liyf@swu.edu.cn

Authors

Xiaoyan Wang − *Key Laboratory of Luminescence Analysis and Molecular Sensing (Southwest University), Ministry of Education, College of Chemistry and Chemical Engineering, Southwest University, Chongqing 400715, P. R. China*

Siyu Xiao − *Key Laboratory of Luminescence Analysis and Molecular Sensing (Southwest University), Ministry of Education, College of Chemistry and Chemical Engineering, Southwest University, Chongqing 400715, P. R. China*

Changping Yang − *Key Laboratory of Luminescence Analysis and Molecular Sensing (Southwest University), Ministry of Education, College of Chemistry and Chemical Engineering, Southwest University, Chongqing 400715, P. R. China*

Congyi Hu − *Key Laboratory of Luminescence Analysis and Molecular Sensing (Southwest University), Ministry of Education, College of Chemistry and Chemical Engineering, Southwest University, Chongqing 400715, P. R. China*

Xue Wang − *Key Laboratory of Luminescence Analysis and Molecular Sensing (Southwest University), Ministry of Education, College of Chemistry and Chemical Engineering, Southwest University, Chongqing 400715, P. R. China*

Shujun Zhen − *Key Laboratory of Luminescence Analysis and Molecular Sensing (Southwest University), Ministry of Education, College of Chemistry and Chemical Engineering, Southwest University, Chongqing 400715, P. R. China*; orcid.org/0000-0003-1236-5501

Complete contact information is available at: https://pubs.acs.org/10.1021/acs.analchem.1c02881

Notes

The authors declare no competing financial interest.

ACKNOWLEDGMENTS

This work was financially supported by the National Natural Science Foundation of China (NSFC, no. 21874109).

REFERENCES

(1) Wang, Y.; Zhao, G.; Chi, H.; Yang, S.; Niu, Q.; Wu, D.; Cao, W.; Li, T.; Ma, H.; Wei, Q. *J. Am. Chem. Soc.* **2021**, *143*, 504−512.
(2) Hu, L.; Xu, G. *Chem. Soc. Rev.* **2010**, *39*, 3275−3304.
(3) Zhang, Y.; Zhao, Y.; Han, Z.; Zhang, R.; Du, P.; Wu, Y.; Lu, X. *Angew. Chem., Int. Ed.* **2020**, *59*, 23261−23267.
(4) Du, D.; Shu, J.; Guo, M.; Haghighatbin, M. A.; Yang, D.; Bian, Z.; Cui, H. *Anal. Chem.* **2020**, *92*, 14113−14121.
(5) Fan, Z.; Lin, Z.; Wang, Z.; Wang, J.; Xie, M.; Zhao, J.; Zhang, K.; Huang, W. *ACS Appl. Mater. Interfaces* **2020**, *12*, 11409−11418.
(6) Wang, Y.; Zhang, Y.; Sha, H.; Xiong, X.; Jia, N. *ACS Appl. Mater. Interfaces* **2019**, *11*, 36299−36306.
(7) Ye, J.; Zhu, L.; Yan, M.; Zhu, Q.; Lu, Q.; Huang, J.; Cui, H.; Yang, X. *Anal. Chem.* **2019**, *91*, 1524−1531.
(8) Liu, Y.; Wang, M.; Nie, Y.; Zhang, Q.; Ma, Q. *Anal. Chem.* **2019**, *91*, 6250−6258.
(9) Huo, X.-L.; Zhang, N.; Yang, H.; Xu, J.-J.; Chen, H.-Y. *Anal. Chem.* **2018**, *90*, 13723−13728.
(10) Zhu, L.; Yu, L.; Ye, J.; Yan, M.; Peng, Y.; Huang, J.; Yang, X. *Biosens. Bioelectron.* **2021**, *178*, 113022.
(11) Zhang, H.-R.; Xu, J.-J.; Chen, H.-Y. *Anal. Chem.* **2013**, *85*, 5321−5325.
(12) Lu, Y.; Ke, H.; Wang, Y.; Zhang, Y.; Li, H.; Huang, C.; Jia, N. *Biosens. Bioelectron.* **2020**, *170*, 112664.
(13) Xiao, S. Y.; Zhen, S. J.; Huang, C. Z.; Li, Y. F. *Biosens. Bioelectron.* **2021**, *186*, 113263.
(14) Zhang, G.; Chai, H.; Tian, M.; Zhu, S.; Qu, L.; Zhang, X. *Anal. Chem.* **2020**, *92*, 7354−7362.
(15) Cai, X.-L.; Zheng, B.; Zhou, Y.; Younis, M. R.; Wang, F.-B.; Zhang, W.-M.; Zhou, Y.-G.; Xia, X.-H. *Chem. Sci.* **2018**, *9*, 6080−6084.
(16) Shang, L.; Wang, X.; Zhang, W.; Jia, L.-P.; Ma, R.-N.; Jia, W.-L.; Wang, H.-S. *Sens. Actuators, B* **2020**, *325*, 128776.
(17) Yin, H.; Shi, Y.; Liu, H.; Dong, Y.; Chu, X. *Microchim. Acta* **2021**, *188*, 181.
(18) Wang, Y.; Shi, H.; Zhang, L.; Ge, S.; Meiling, X.; Wang, X.; Yu, J. *J. Hazard. Mater.* **2021**, *403*, 123601.
(19) Han, Z.; Shu, J.; Jiang, Q.; Cui, H. *Anal. Chem.* **2018**, *90*, 6064−6070.
(20) Gu, W.; Wang, H.; Jiao, L.; Wu, Y.; Chen, Y.; Hu, L.; Gong, J.; Du, D.; Zhu, C. *Angew. Chem., Int. Ed.* **2020**, *59*, 3534−3538.
(21) Xiao, S. Y.; Li, Y.; Zhen, S. J.; Huang, C. Z.; Li, Y. F. *Electrochim. Acta* **2020**, *357*, 136842.
(22) Gui, G.-F.; Zhuo, Y.; Chai, Y.-Q.; Xiang, Y.; Yuan, R. *Anal. Chem.* **2014**, *86*, 5873−5880.

(23) Zhu, D.; Zhang, Y.; Bao, S.; Wang, N.; Yu, S.; Luo, R.; Ma, J.; Ju, H.; Lei, J. *J. Am. Chem. Soc.* **2021**, *143*, 3049−3053.
(24) Voci, S.; Duwald, R.; Grass, S.; Hayne, D. J.; Bouffier, L.; Francis, P. S.; Lacour, J.; Sojic, N. *Chem. Sci.* **2020**, *11*, 4508−4515.
(25) Yan, M.; Xin, J.; Fan, L.; Ye, J.; Xiao, T.; Huang, J.; Yang, X. *Anal. Chem.* **2021**, *93*, 3461−3469.
(26) Jiang, Z. W.; Zou, Y. C.; Zhao, T. T.; Zhen, S. J.; Li, Y. F.; Huang, C. Z. *Angew. Chem., Int. Ed.* **2020**, *59*, 3300−3306.
(27) Yang, C. P.; He, L.; Huang, C. Z.; Li, Y. F.; Zhen, S. J. *Talanta* **2021**, *221*, 121498.
(28) Zhou, J.; Li, Y.; Wang, W.; Tan, X.; Lu, Z.; Han, H. *Biosens. Bioelectron.* **2020**, *164*, 112332.
(29) Liao, X.; Fu, H.; Yan, T.; Lei, J. *Biosens. Bioelectron.* **2019**, *146*, 111743.
(30) Zhou, Y.; He, J.; Zhang, C.; Li, J.; Fu, X.; Mao, W.; Li, W.; Yu, C. *ACS Appl. Mater. Interfaces* **2019**, *12*, 338−346.
(31) Shi, L.; Sun, Y.; Mi, L.; Li, T. *ACS Sens.* **2019**, *4*, 3219−3226.
(32) Sun, Y.; Wang, Q.; Mi, L.; Shi, L.; Li, T. *Anal. Chem.* **2019**, *91*, 12948−12953.
(33) Xiao, B.; Zhao, X.; Huang, C.; Li, Y. *Mater. Lett.* **2015**, *152*, 139−141.
(34) Li, Y.; Chu, Y.; Li, Y.; Ma, C.; Li, L. *Sens. Actuators, B* **2020**, *303*, 127222.
(35) Li, Y.; Huang, C. Z.; Li, Y. F. *Anal. Chem.* **2019**, *91*, 9308−9314.
(36) Li, Y.; Jiang, Z. W.; Xiao, S. Y.; Huang, C. Z.; Li, Y. F. *Anal. Chem.* **2018**, *90*, 12191−12197.
(37) Yang, J.; Hu, R.-X.; Zhang, M.-B. *J. Solid State Chem.* **2012**, *196*, 398−403.
(38) Cao, Y.; Zhu, W.; Wei, H.; Ma, C.; Lin, Y.; Zhu, J.-J. *Anal. Chem.* **2020**, *92*, 4123−4130.
(39) Tan, X.; Zhang, B.; Zou, G. *J. Am. Chem. Soc.* **2017**, *139*, 8772−8776.
(40) Wang, T.; Wang, D.; Padelford, J. W.; Jiang, J.; Wang, G. *J. Am. Chem. Soc.* **2016**, *138*, 6380−6383.
(41) Hu, Q.; Su, L.; Mao, Y.; Gan, S.; Bao, Y.; Qin, D.; Wang, W.; Zhang, Y.; Niu, L. *Biosens. Bioelectron.* **2021**, *178*, 113010.
(42) Zou, R.; Teng, X.; Lin, Y.; Lu, C. *Trends Anal. Chem.* **2020**, *132*, 116054.

https://doi.org/10.1021/acs.analchem.1c02881
Anal. Chem. 2021, 93, 14178−14186